Research on 3D FBG accelerometer and demodulation method

Qiuming Nan (南秋明)[1,2]* and Lei Song (宋 蕾)[3]

[1]*National Engineering Laboratory for Fiber Optic Sensing Technology, Wuhan University of Technology, Wuhan 430070, China*

[2]*Key Laboratory of Fiber Optic Sensing Technology and Information Processing, Ministry of Education, Wuhan University of Technology, Wuhan 430070, China*

[3]*School of Electronic and Information Engineering, LiaoNing University of Science and Technology, Anshan 114021, China*

**Corresponding author: 197114012@qq.com*

In order to meet the requirements of vibration monitoring of large mechanical equipment, the authors design a novel three-dimensional (3D) high-frequency fiber Bragg grating (FBG) accelerometer. First, the operation principle of the sensor is introduced; the theoretical calculation and finite element analysis are performed about its structural parameters in this paper. Second, an FBG demodulation method for vibration signal is studied and a compensation method is put forward to measure the error caused by fluctuation of the light source and line loss. Finally, sensing properties such as amplitude frequency characteristics, sensitivity of the sensor, crosstalk coefficient, space acceleration measurement are tested, and the compensation method for measurement error is validated. The results show that the operating frequency bandwidth of the transducer is 10500 Hz, sensitivity is about 1400 mv/g, crosstalk coefficient is larger than 20.6 dB, and the maximum measurement error of space acceleration is 4.8%, the compensation error is less than 5%. Hence, the sensor is used to monitor the vibration state of mechanical equipment.

OCIS codes: 230.0230, 250.0250, 260.0260.
doi: 10.3788/COL201412.S12302.

Vibration monitoring is one of the most effective methods in mechanical equipment monitoring and fault diagnosis field. The vibration monitoring mainly uses the electromagnetic vibration sensors, such as piezoelectric sensor. Although the technology is well-developed with excellent performance, its disadvantages are poor ability to resist electromagnetic interference, signal not transmitted over long distance, difficult to achieve large-scale network. So, it is difficult to realize real-time and large-scale monitoring for the vibration state of mechanical equipment in the flammable, explosive and electromagnetic interference situation[1,2]. Owing to many advantages of fiber Bragg grating (FBG) technology, since the emergence in late 70's, though it has aroused a great concern, it has been developing very rapidly. After 2000, research and application of the technology have started in the vibration monitoring of mechanical equipment, and resulted in a few achievements[3,4]. But the existing FBG accelerometers are largely one-way, unable to meet the needs of three-dimensional vibration measurement.

Then if one-way accelerometer is used, it requires at least three accelerometers for better functionality, which increases the cost of testing. Often, because of the installation space constraint, multiple sensors cannot be installed in the same monitoring point; eventually, testing data cannot reflect the real acceleration value in different directions of the monitoring point. However, so far, reports of 3D FBG accelerometer are rare; there is no report especially on 3D FBG accelerometer used in vibration monitoring of mechanical equipment. Hence,

the research on the sensor is the focus of the paper[5–7].

In addition, in order to solve the problem of vibration signal demodulation speed, a light intensity demodulation method is adopted based on matched filter. But the method has one obvious disadvantage, namely, low measurement accuracy, which is caused by attenuation of light source and line loss. Solving of this problem is also considered in this paper.

Figure 1 shows the 3D FBG accelerometer studied in this paper, which is composed of three unidirectional sensing units that are mutually vertical. Each sensing unit is composed of a base, an elastomer, a mass block and two FBGs, and its structure and principle are shown in Fig. 2. Two FBGs written in the same optical fiber are formed into precise matching by accurate fabrication process, and they are symmetrically fixed between the base and the mass block. In order to avoid dead zone, they are pre-stretched about 1 nm. When the sensor receives the vibration signal from the outside world, the mass supported by the elastic membrane vibrates up and down in order to drive the FBGs axial expansion, envelope area of reflection peaks of FBG1; and FBG2
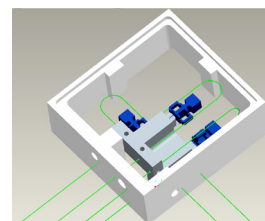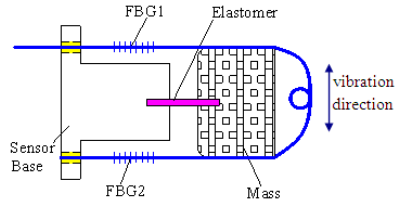

Fig. 1. Structure of 3D FBG accelerometer.

Fig. 2. Structure and principle of sensing unit.

changes, as shown in Fig. 3. The envelope area is proportional to the intensity of reflection spectrum. To take the upward acceleration of the mass block as an example, FBG2 elongates, FBG1 shrinks, and light-intensity signal detected by photoelectric detector increases, and vice versa.

In order to further illustrate the working principle of the sensor, the authors have conducted theoretical calculation and finite element analysis. As shown in Fig. 4, the upward exciting force exerted to mass block is, $F_a = ma$, and it makes the elastomer deform, while FBG2 is elongated to generate a left tension F_f. For the elastomer, the stress state can be transformed into equivalent to force F_a and a clockwise torque $M = F_f \times d$, where d is the distance between mass block and elastic node, namely the distance between A and B in Fig. 4.

According to the calculation of mechanics of materials for the deformation of bending beam, the deflection ω of elastic body can be expressed as

$$\omega = \frac{F_a l^3}{3EI} - \frac{M l^2}{2EI}, \tag{1}$$

where, l is the length of the elastomer, E is the elastic modulus, I is the moment of inertia.

$$\Delta L = O'A' - O'A =$$
$$\sqrt{\left(O'A + A'B' \sin\alpha\right)^2 + \left(AB + BB' - A'B' \cos\alpha\right)^2} - O'A. \tag{2}$$

The tension ΔL of the optical fiber subjected to external vibration can be expressed as Eq. (2), as shown in Fig. 4, α is angle of the elastomer caused by stress. As the rotation angle is very small, Eq. (2) can be
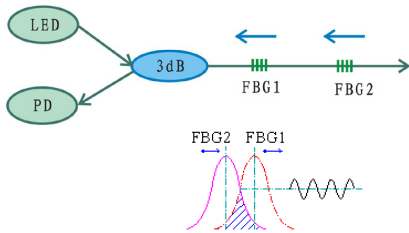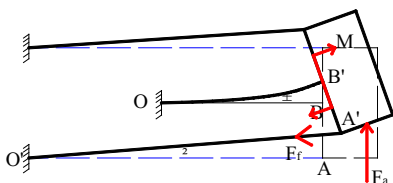

Fig. 3. Matching demodulation principle.

Fig. 4. Schematic diagram of the force exerted to the sensor.

expressed as

$$\Delta L = \sqrt{L^2 + \omega^2} - L = \omega, \tag{3}$$

where, L is the original length of the fiber.

The axial stress of fiber and the change in wavelength caused by the stress can be expressed, respectively, as

$$F_f = \sigma A = \varepsilon E_f A = \frac{\Delta L}{L} E_f A = K_f \Delta L, \tag{4}$$

$$\Delta\lambda = (1 - P_e)\lambda\varepsilon. \tag{5}$$

From simultaneous Eqs. (1)–(5), the sensitivity of the sensor can be expressed as

$$S = \frac{\Delta\lambda}{a} = \left(1 - P_e\right)\lambda \frac{1}{L} \frac{2ml^2}{6EI + 3K_f dl^2}. \tag{6}$$

From Eq. (6), it can be observed that there is a linear relationship between the wavelength change of FBG and the outside acceleration.

The elastomer can be regarded as a uniform cantilever beam, its stiffness is expressed as

$$K_e = \frac{3EI}{l^3}. \tag{7}$$

According to the kinematics equation of object structure, the first-order resonant frequency of the sensor is calculated as

$$f = \frac{1}{2\pi}\sqrt{\frac{K}{m}} = \frac{1}{2\pi}\sqrt{\frac{K_e + \left(d/L\right)^2 K_f}{m}}. \tag{8}$$

In addition to the theoretical calculation, the authors have verified the upper theoretical formula of sensor structure by using the finite element analysis method, which guides next experiment. Figure 5 shows the first-order mode of the sensor. Result of finite element analysis shows that the first-order mode frequency of the sensor is about 1000 Hz; and the subsequent experiment shows that the result is in agreement with the experimental result.

In order to obtain high-speed demodulation for fiber optic vibration signal, this paper adopts matched fiber grating demodulation method. It realizes wavelength demodulation by judging the intensity of the reflected light. As the light intensity can be directly detected by photoelectric detector, eliminating costly F-P filters significantly reduces the production cost.

At the same time, the conversion speed of photoelectric conversion module is so fast that intensity demodulation can have a faster speed than wavelength demodulation[8,9]. As two matching FBGs are in the same environment, the problem of temperature compensation is easily solved.

However, light intensity detection is susceptible to interference and has low precision because it is difficult to keep light source stable, and leads to loss with the passage of time. In addition, transmission loss of optical
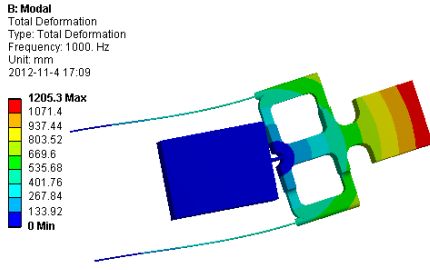
Fig. 5. First-order mode of the sensor.

fiber cable in use is unpredictable; these adverse factors affect the detection accuracy, and interfering signal may submerge detection signal. Therefore, in order to apply intensity demodulation solution in practical engineering, the problem of intensity demodulation method affected by fluctuation of light source power and line loss must be solved.
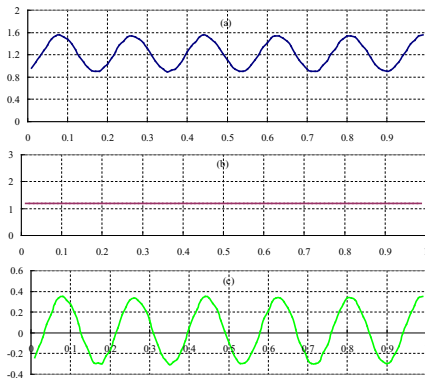
As shown in Fig. 6, when the acceleration sensor is static (i.e., acceleration is 0), envelope area of reflection peaks of the sensing optical gratings is S; at this time, after the photoelectric conversion, in the output voltage waveform [as shown in Fig. 6(b)], the voltage V_1 is kept constant, namely, the voltage waveform is a horizontal line parallel to the X-axis. The sinusoidal vibration and envelope area are changed to avail $S \pm \Delta S$. At this time, after the photoelectric conversion, the output of voltage waveform is as shown in Fig. 6(a). The voltage waveform is found to be equivalent to the synthesis of DC voltage and AC voltage (sinusoidal). If the DC signal is separated from AC signal, the AC voltage V_2 can be obtained and its voltage waveform is shown in Fig. 6(c).

DC voltage V_1 can be expressed as

$$V_1 = K_1 \rho S, \tag{9}$$

where, K_1 is the coefficient relevant to optical power fluctuation, ρ is light density of broadband light source, which is a fixed value. S is the envelope area of reflection peak of sensing optical gratings in static state, which is decided by the initial matching state of the sensor; for the same sensor, this value is fixed.

AC voltage V_2 obtained by the vibration signal of acceleration a can be expressed as

Fig. 6. (a) Synthetic waveform of AC and DC, (b) waveform of DC V_1, and (c) waveform of AC V_2.

$$V_2 = K_1 \rho \Delta S = K_\alpha \alpha, \tag{10}$$

where ΔS is the change in envelope area S caused by vibration signal proportional to the vibration acceleration a.

With the light attenuation or line loss, optical power fluctuation coefficient is represented as K_1 and the DC voltage V_1 at this time can be expressed as

$$V_1' = K_1' \rho S. \tag{11}$$

When the acceleration a is unchanged, the AC voltage V_2' at this time can be expressed as

$$V_2' = K_1' \rho \Delta S = K_\alpha' \alpha. \tag{12}$$

From Eqs. (9)–(12),

$$K_\alpha' = \frac{V_1'}{V_1} K_\alpha. \tag{13}$$

As Eq. (13) shown, when the DC voltage is V_1, corresponding calibration coefficient of acceleration sensor is K_α. When there is light attenuation or line loss, DC voltage changes from V_1 to V_1', the calibration coefficient changes from K_α to K_α'. As long as V_1 and V_1' are measured, the calibration coefficient K_α can be modified and a corrected coefficient K_α' can be obtained. With this dynamic compensation, we can measure the acceleration value in case of light attenuation or line loss precisely.

Functions of 3D FBG accelerometer mainly include amplitude–frequency response, sensitivity calibration, cross-talk coefficient and space acceleration measurement. Figure 7 shows experimental devices, which include LAN-XI vibration analysis system, vibration exciter type 4808, power amplifier type 2719 and standard reference acceleration sensor (type 4371) (Danish B&K company). The sensor is fixed through the mounting bracket on the B&K vibration test platform using the output parameter PULSE control to adjust the vibration system.

In the amplitude frequency characteristic test, the exciter is adjusted to constant acceleration 3 m/s^{-2} as the input signal; the frequency of input signal starts from 10 Hz, increasing 50 Hz in each step; when the frequency reaches 800 Hz, 20 Hz is increased in each step. During the test, we observed that the change in the output voltage value determines the natural frequency and frequency-measuring range. The amplitude–frequency characteristics of three sensing units (X, Y and Z) are measured, as shown in Fig. 8. The results show that
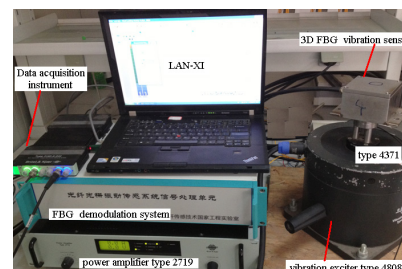

Fig. 7. Optical fiber vibration testing system.

the first-order resonant frequencies of three sensing units are 910, 890 and 890 Hz, respectively; curve flat segment ranged from 10 to 500 Hz; and the operating frequency range of the sensor is 10–500 Hz.

The difference between the experimental result of amplitude frequency characteristics and the result of finite element analysis is mainly because the contact in various components of the finite element analysis is automatically defined as a complete contact. However, in fact, there is always a gap in various components caused by various conditions when the components of the sensor are in the assembly, which result in the actual stiffness of assembly sensor lower than the structure stiffness in finite element analysis, with which the experimental value of first-order resonance frequency becomes lower than the analysis value.

Linear calibration experiment measures sensitivity, linearity and linear measurement range of the accelerometer. The frequency of the input signal is 200 Hz, and measurement acceleration is within 0.1–1 g, which is read out by the piezoelectric standard acceleration sensor, type 4371. The output voltage values of 3D FBG accelerometer in each acceleration value are noted down. Figure 9 shows the calibration curves, in which we can observe that when the input acceleration is within 0–0.5 g, the linear degrees of calibration curves are all more than 0.999; and the linear sensitivities of three sensing units are 145 mv/ms^{-2}, 138 mv/ms^{-2}, 150 mv/ms^{-2}, respectively. With an increase in the acceleration, the output voltage increases slowly, and the sensitivity decreases; when the acceleration is more than 0.8 g, the output voltage becomes saturated. Therefore, the linear measurement range of the sensor is 0–0.5 g, which is determined by the tunable linear interval of matching gratings.

The acceleration sensing system is a vector sensing system, and the direction of the response is an important and unique performance. This paper introduces the crosstalk coefficient (CC) to measure the direction-
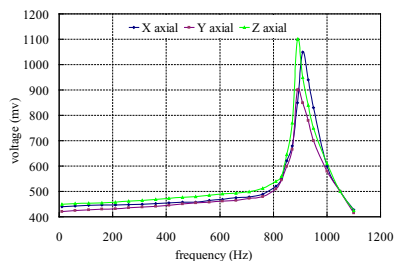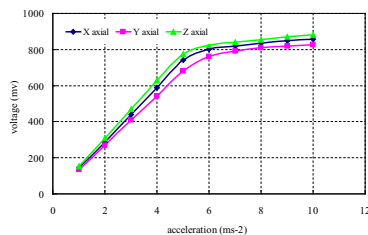

Fig. 8. Amplitude–frequency characteristic curves.

Fig. 9. Calibration curve of 3D FBG accelerometer.

Table 1. Test results of crosstalk coefficient (mv)

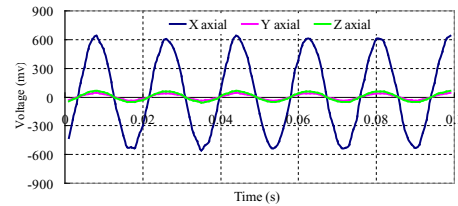| Main vibration direction		x	y	z
Output response	x	450	36	38
	y	32	462	39
	z	34	35	470

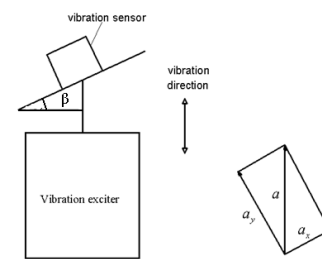Fig. 10. Vibration response curves of X axial, Y axial and Z axial as the X axial is the main direction of vibration.

Fig. 11. Measurement method of space acceleration.

Table 2. Space acceleration measurement and verification, input acceleration is 2 ms^{-2}

Angle β		**30°**	**45°**	**60°**
Measured data	α_x	0.98	1.36	1.69
	α_y	1.65	1.41	1.01
	α_z	0.1	0.12	0.11
	α	1.92	1.98	1.97

Table 3. Space acceleration measurement and verification, input acceleration is 5 ms^{-2}

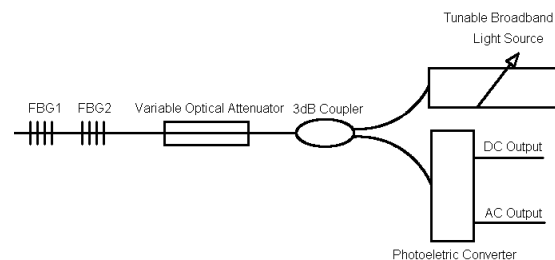| Angle β		**30°**	**45°**	**60°**
Measured data	α_x	2.45	3.42	4.57
	α_y	4.08	3.51	2.18
	α_z	0.19	0.17	0.21
	α	4.76	4.9	5.11

Fig. 12. Diagram of the compensation scheme of measuring error.

Table 4. Experimental results in four different conditions

Working condition	DC voltage	AC voltage	Calculated value by formula(13)	Compensation error
No decay, no loss	1200	450		
10% attenuation	1068	405	401	0.99%
3Db loss	580	213	218	-2.29%
10% attenuation and 3Db loss	520	198	195	1.54%

al response effect of 3D FBG accelerometer. Crosstalk coefficient is defined as

$$CC = 20 \log\left(\frac{S_{axial}}{S_{cross}}\right). \tag{14}$$

Let the vibration direction of the exciter be X-axis, the input signal a sine wave signal, vibration frequency 60 Hz, vibration acceleration 3 m/s^{-2}, the simultaneous acquisition for response of three directions, X, Y, and Z axes, response waveform as shown in Fig. 10, and the effective values of output voltage are 450, 32 and 34 mV, respectively. Similarly, under invariable vibration signal condition, Y and Z axis are considered as main vibration directions and the above experiments are repeated. The results are shown in Table 1. According to Eq. (14), crosstalk coefficient calculated to be 20.6 dB. Thus, it is understood that the sensor has good direction, and crosstalk has little effect on the measurement.

In order to test the feasibility and accuracy of 3D FBG accelerometer for measuring space acceleration, the design of the experiment scheme is shown in Fig. 11. The vibration direction of vibration exciter in the plot is vertical, and the 3D FBG accelerometer is installed on the bracket with an angle β to a horizontal plane. At this time, the angles between the measuring directions (X, Y and Z axes) and the actual vibration direction are (90°$-\alpha$), α, 90°, respectively; therefore, the vibration signal has vibration components in the direction of X and Y axes of the sensor, but the vibration component in Z axis should be 0.

During the experiment, the vibration frequency is 200 Hz, the input acceleration is from the standard acceleration sensor, and acceleration components are measured by 3D FBG accelerometer. By setting different tilt angles of bracket and changing the input acceleration, we get multiple group data, shown in Tables 2 and 3. From the data in the tables, the synthesis of output components of X, Y and Z axes is basically the same as the input acceleration, and the maximum error is only −4.8%. This shows that the sensor has higher precision in measuring space acceleration.

In order to verify the above compensation method of measurement of error caused by attenuation of light source and line loss, some simulation experiments are carried out. In order to simulate the light attenuation, a tunable broadband light source is used in the FBG demodulator. In order to simulate line loss of the light, a 3-dB optical attenuator is used in the optical path of the experimental system, as shown in Fig. 12. Experiments are carried out in four different conditions, but in the processes, the vibration direction is always X axis and the input acceleration value remains unchanged at 3 ms^{-2}. Experimental results are shown in Table 4.

It can be seen from Table 4 that in the conditions of attenuation or loss, the measured value of AC voltage is very close to the calculated value according to Eq. (13), and the maximum error is only −2.29%. Hence, it can be concluded that the compensation method has high precision.

Aiming at the demands for the vibration state monitoring of large mechanical equipment, a novel 3D high-frequency FBG accelerometer is developed. Advantages of this sensor are strong ability of anti-electromagnetic interference, intrinsic safety, long-distance transmission of signal and good stability. Results of experimental researches show that the operating frequency of the sensor in three directions is in the range of 10–500 Hz, acceleration measurement range is 0–0.5 g, linear sensitivity is about 1400 mV/g, the crosstalk coefficient is more than 20.6 dB, and the sensor is used to measure space acceleration. In addition, FBG demodulation method for vibration signal is studied, and a compensation method is put forward and verified by the experiment.

In conclusion, the performance of the 3D FBG accelerometer is good. It is further improved in terms of its frequency and acceleration measurement range for broad application prospects.

References
1. Y. Z. Zheng, Gas Tribine Power Gener. Technol. **12,** 199 (2010).
2. D. N. Fu, Mach. Tool Hydraul. **1,** 152 (2005).
3. D. S. Zhang, Chin J. Sci. Instrum. **30,** 1401 (2009).
4. P. Luo and J. W. Tian, Opto-Electron. Eng. **39,** 25 (2012).
5. Y. T. Zhao and Z. Q. Li, Chin. J. Sci. Instrum. **27,** 300 (2006).
6. Z. Yang, Sci. Technol. Eng. **9,** 3201 (2009).
7. J. H. Wang, Chin. J. Sensors Actuators **19,** 805 (2006).
8. C. G. Lu, Chin. J. Sensors Actuators **20,** 859 (2007).
9. L. W. Ding, Electro-Optic Technol. Appl. **24,** 38 (2009).